JGR Space Physics

RESEARCH ARTICLE
10.1029/2023JA032203

Key Points:

- Superposed epoch analysis shows dynamic evolution of O^+ ions during geomagnetic storms
- Significant enhancement of the O^+-to-H^+ number density ratio observed at radial distances less than 12 R_E
- Scalar temperature for both species show the arrival of heated ions far from Earth throughout the analyzed period

Correspondence to:
L. H. Regoli,
Leonardo.Regoli@jhuapl.edu

Citation:
Regoli, L. H., Gkioulidou, M., Ohtani, S., Raptis, S., Mouikis, C. G., Kistler, L. M., et al. (2024). Temporal evolution of O^+ population in the near-Earth plasma sheet during geomagnetic storms as observed by the magnetospheric multiscale mission. *Journal of Geophysical Research: Space Physics*, *129*, e2023JA032203. https://doi.org/10.1029/2023JA032203

Received 20 OCT 2023
Accepted 28 MAR 2024

Author Contributions:
Formal analysis: L. H. Regoli, M. Gkioulidou, S. Ohtani, C. G. Mouikis
Funding acquisition: M. Gkioulidou
Investigation: L. H. Regoli, M. Gkioulidou
Methodology: L. H. Regoli, L. M. Kistler
Project administration: M. Gkioulidou
Software: L. H. Regoli
Writing – original draft: L. H. Regoli
Writing – review & editing: M. Gkioulidou, S. Ohtani, S. Raptis, L. M. Kistler, I. J. Cohen, S. A. Fuselier

Temporal Evolution of O^+ Population in the Near-Earth Plasma Sheet During Geomagnetic Storms as Observed by the Magnetospheric Multiscale Mission

L. H. Regoli[1], M. Gkioulidou[1], S. Ohtani[1], S. Raptis[1], C. G. Mouikis[2], L. M. Kistler[2], I. J. Cohen[1], and S. A. Fuselier[3,4]

[1]Johns Hopkins University Applied Physics Laboratory, Laurel, MD, USA, [2]Space Science Center, University of New Hampshire, Durham, NH, USA, [3]Southwest Research Institute, San Antonio, TX, USA, [4]University of Texas at San Antonio, San Antonio, TX, USA

Abstract During geomagnetic storms, the increase in energy input into the ionosphere in the form of Poynting flux and electron precipitation leads to an enhanced ionospheric outflow that results in an increase of the O^+ content in the magnetosphere. Using different missions and instrumentation, two main ionospheric sources have been identified for the oxygen ions reaching the inner magnetosphere during geomagnetic storms: the dayside cusp, and the night side auroral region. Evidence of both pathways have been presented in the literature. However, the relative contribution of each of these pathways to the enhancement of O^+ observed in near-Earth plasma sheet, as well as the dynamics involved during the development of geomagnetic storms remains an open question. Here, we present the first statistical study to date to address this question, in the form of a superposed epoch analysis of O^+ and H^+ moments obtained by the Magnetospheric Multiscale (MMS) mission throughout the main phase of 90 geomagnetic storms with a minimum SYM-H of at least −50 nT. The results show a clear increase in the oxygen density in the near-Earth plasma sheet, with values further from Earth remaining low. Temperature values for both species show an increase with the progress of the storms. These results combined suggest that, during the main phase of geomagnetic storms, most of the oxygen ions observed in the near-Earth plasma sheet are traveling directly from the nightside auroral region.

1. Introduction

The enhancement of O^+ fluxes in the ring current during geomagnetic storms has been extensively documented in the literature (e.g., Hamilton et al., 1988; Kistler et al., 1989; Zhao et al., 2015). These ions can originate from the dayside cusp or the nightside auroral region (e.g., Kronberg et al., 2014). The initial acceleration that leads to escape can occur through several different mechanisms that take place at different altitudes in the ionosphere (Maggiolo, 2015). Due to the magnetospheric configuration, outflowing ions originated at the dayside cusp have been observed to travel along field lines that are convecting toward the nightside, and they reach the plasma sheet at different radial locations with different energies, due to a velocity filter effect (Kistler et al., 2019). Once these ions reach the plasma sheet, they are transported earthward and eventually, depending on their energy, reach the ring current. This earthward transport can happen due to convection (Lui, 1991), which is enhanced during active times, or through bursty bulk flows (Angelopoulos et al., 1992; Pitkänen et al., 2023). On the other hand, ions originated at the nightside auroral region can have a more direct access to the near-Earth plasma sheet and inner magnetosphere by traveling directly along closed field lines.

The dynamics of storm-time ions in the magnetosphere have been analyzed during the last couple of decades using different spacecraft and different instrumentation. Using energetic neutral atom (ENA) data from the IMAGE/HENA instrument, Mitchell et al. (2003, 2005) analyzed the enhancements of H^+ and O^+ during storm-time, and found an increase in the 52–180 keV O^+ content in the ring current that appears a few hours after the enhancement in 27–120 keV H^+, that occurs almost immediately after sudden commencement. Analyzing the response of both species to the occurrence of storm-time substorms, they found that, after O^+ is present in the magnetosphere, enhancements in the O^+ fluxes are well correlated with substorm onset.

Kistler et al. (2010) analyzed three separate storms using data from the Cluster spacecraft, and showed the acceleration and transport of O^+ ions originated on the dayside cusp into the plasma sheet and subsequently to the ring current. In their observations, the enhanced outflow was particularly evident in the lobes at a distance of

approximately ~20 R_E. Cluster's polar orbit with apogee at approximately 19 R_E does favor the observation of ions coming from the dayside cusp, but makes it difficult to detect ions in the near-Earth plasma sheet that originate from the nightside auroral oval.

Using Geotail data, Ohtani et al. (2011) performed a statistical analysis of ion characteristics in the plasma sheet without distinction of geomagnetic activity levels. They found that, while the H^+ and O^+ number densities follow the expected trend, with density increasing with decreasing radial distance, their mean energy differ, with that of H^+ increasing with decreasing radial distance, but that of O^+ following an opposite trend. They interpreted this result as an indication that an important part of the O^+ detected in the near-Earth plasma sheet (closer than 10 R_E) has not been accelerated through transport from the distant tail, and thus must be reaching that region through a more direct access from the nightside ionosphere. Ohtani et al. (2011) also analyzed the trend in the same quantities for different levels of solar and geomagnetic activity, but they did not demonstrate how these quantities evolve during the course of geomagnetic storms.

More recently, Kistler et al. (2019) analyzed a specific event combining data from the Magnetospheric Multiscale (MMS) and Arase spacecraft, where they identified two different O^+ populations entering the plasma sheet. Based on the energy characteristics of both populations and where they are observed, as well as the presence of energy dispersions and the bursty nature of one of the observed populations, they concluded that one of the populations originated in the dayside cusp, traveling through the plasma sheet boundary layer, while the other one originated in the night side auroral region, observed in the plasma sheet.

Gkioulidou et al. (2019) analyzed a bidirectional O^+ ion outflow event detected by Van Allen Probes, reaching the inner magnetosphere at $L \sim 4$. Field-aligned Poynting flux enhancements were observed associated with the event, indicating electromagnetic heating of the atmosphere leading to ion outflow, similar to what was observed by Strangeway et al. (2005). Using a 2-D guiding center test particle model, Gkioulidou et al. (2019) attributed the origin of these ions to both hemispheres of the nightside ionosphere. Statistical studies, using Van Allen Probes data, also showed that these ions go directly into the inner magnetosphere are associated with AE-index enhancements, and magnetic field dipolarization (Liu & Zong, 2022; Nosé et al., 2016).

Despite all the existing literature, the relative contribution of each mechanism for ionospheric plasma to access the current sheet close to Earth during geomagnetic storms remains poorly understood. The low-latitude, elliptical orbit of MMS provides a possibility to observe the evolution of the O^+ populations close to the plasma sheet in a statistical manner. In this paper, we present the first superposed epoch analysis of O^+ and H^+ moments throughout the main phases of 90 geomagnetic storms. Our results shed new light on the source and evolution of the O^+ ion population during the course of geomagnetic storms.

This paper is organized as follows. Section 2 presents a summary of the instrumentation used for the statistical analysis. Section 3 provides a description of the statistical analysis performed. Section 4 presents the results of the analysis. Finally, Section 5 presents the conclusions derived from the analysis.

2. Instrumentation

In order to understand the temporal evolution of O^+ ions during geomagnetic storms, we use data from the Hot Plasma Composition Analyzer (HPCA, Young et al., 2016) onboard the MMS 1 spacecraft, as well as the SYM-H index provided by OMNIWeb. The SYM-H index is derived by subtracting the geomagnetic field and solar quiet variation from the data obtained by six ground-based magnetic stations.

HPCA combines an electrostatic analyzer with time-of-flight measurements to provide ion energy (~1 eV to 40 keV) and composition information ($M/\Delta M \sim 4$) with a time resolution of 10 s (half a spacecraft spin period). HPCA also provides 3-D distributions of major ion species (H^+, He^{++}, He^+, and O^+). For this study, we are primarily concerned with H^+ and O^+, and for the analyses presented we use moments data, specifically number density and scalar temperature, both obtained from level 2 HPCA data from the MMS SDC. HPCA is not capable of distinguishing between N^+ and O^+ ions, so even when O^+ is expected to be dominant, some N^+ (also of ionospheric origin) will inevitably contribute to the measurements reported in this study.

Throughout most of the duration of the MMS mission, the HPCA instrument applied an on-board data compression algorithm that resulted in the elimination of single counts for each energy-angle-angle bin. When considering the spin-averaged ion fluxes, these single counts can add up to a non-negligible amount of oxygen

that was not accounted for by the data returned by HPCA. As a result of this data compression, for most of the data available during the period covered in this study (with the exception of a few months in 2018 and 2019, during which a corrected compression algorithm was uploaded to the spacecraft) the instrument detected lower fluxes of oxygen than were actually present in the magnetosphere. The flux corresponds to the counts divided by the central energy of the bin, and thus this affects more strongly the fluxes detected at the lowest energies.

In principle, such a compression algorithm underestimates the O^+ densities for times when the fluxes are not particularly high, which means that comparing time periods with two different compression algorithms could yield skewed results. For this reason, we evaluated the difference in the results presented in the next section excluding the data collected when the algorithm was corrected, and including it. The results do not vary significantly, and for that reason we decided to include all the data, regardless of the compression algorithm being used, since this improves the statistics of the analysis presented here.

Due to the fact that in general there is more H^+ than O^+ in the magnetosphere, the compression algorithm mentioned above has a stronger effect in the measured oxygen ion densities compared to protons. When analyzing the ion densities (Section 4.1), we focus on O^+ to H^+ density ratios, so the resulting ratios will represent lower limits of what is actually present in the plasma sheet during geomagnetic storms, but the observed trends should not be affected by it. On the other hand, since the scalar temperatures for O^+ (Section 4.2) correspond to the mean energy of the distribution, these are expected to be affected as well, being shifted to larger values, due to the elimination of the lower energy ions from the overall detected population.

Figure 1 shows data from the MMS 1 spacecraft and the SYM-H index obtained from the OMNI dataset (panel a) during a storm that took place in July 2017. This event corresponds to one of the storms included in the statistical analysis presented in the next section, where O^+ access is observed in the near-Earth plasma sheet. Panels b and c show ion spectrograms for H^+ and O^+ as measured by HPCA respectively. Prior to the beginning of the main phase of the storm, HPCA detected almost no O^+, and an H^+ population with a broad energy band centered at around 2 keV. Soon after the beginning of the main phase, there is an enhancement in the H^+ fluxes with a similar energy, as well as the appearance of a lower-energy population with lower fluxes (at energies less than 500 eV). At the same time, a lower energy O^+ population appears, reaching a peak at roughly two and a half hours after the beginning of the main phase, when the O^+ contribution to the total density almost matches that of H^+, as visible in panel *e*, showing the ratio of O^+ to H^+ number density.

Panel d shows pitch angle distribution for O^+. The energies covered by this panel correspond to the main O^+ population observed in panel c. The pitch angle distribution shows a population traveling along the field line for most of the time period shown (highlighted by the vertical dashed lines), indicating ions reaching the low latitudes from the northern-hemisphere ionosphere, except for a period showing flows traveling in both direction, possibly a combination of a reflected population or ions coming directly from the southern-hemisphere ionosphere, and the ions being isotropized when entering the plasma sheet. The last panel (panel g) shows the plasma beta (with the dashed horizontal line showing the boundary of 0.2 used to identify transition between lobes and plasma sheet), indicating that MMS 1 was flying around the plasma sheet at the time of the event, with some excursions into the lobes. For this particular event, the O^+-to-H^+ density ratio is increase, although O^+ never gets to dominate the plasma sheet contents.

Figure 2 shows another event, with the same panels from Figure 1, but for a geomagnetic storm that took place in July 2022. In this occasion, MMS observed O^+ ions entering the distant tail. During this event, MMS is going in and out of the plasma sheet, and a bi-directional flow of O^+ ions can be observed prior to the beginning of the storm and during the main phase (highlighted by the two pairs of vertical dashed lines). During the main phase of the storm, the observed O^+ population is predominantly field-aligned, accessing the plasma sheet from the southern hemisphere. Additionally, an increase in the O^+-to-H^+ density ratio is observed traveling tailwards on the southern lobe and the plasma sheet boundary layer. This increase reaches the point where O^+ ions dominate over H^+.

3. Statistical Analysis

For the analysis presented here, we make use of data returned by the MMS 1 spacecraft between January 2016 and December 2022. The analysis focuses on times when a geomagnetic storm with a minimum SYM-H index of at least −50 nT was taking place. In total, 90 geomagnetic storms with these characteristics occurred during this time period.

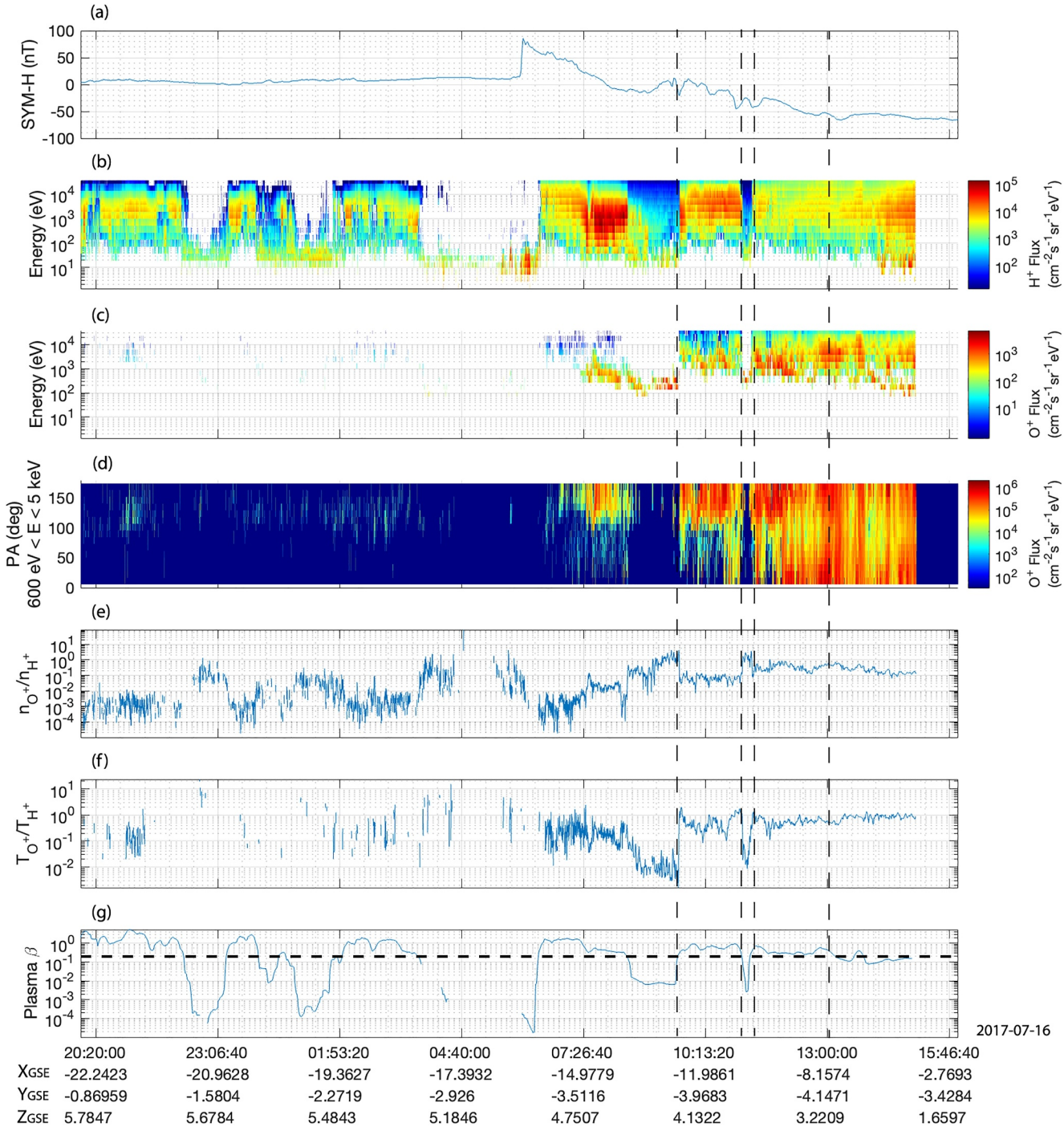

Figure 1. Data obtained during a geomagnetic storm that took place on 16 July 2017. Panel a shows the SYM-H index from the OMNI data; panels b and c show the H^+ and O^+ flux spectrograms from MMS1/HPCA; panel d shows the pitch angle distribution for O^+ for energies between 600 eV and 5 keV; panels e and f show the O^+-to H^+ density and temperature ratios; panel *g* shows the plasma beta, with the horizontal dashed line showing the boundary of 0.2 used to define the transition between plasma sheet and the lobes.

Since our main interest is in the evolution of the O^+ population in the tail and plasma sheet during geomagnetic storms, we reduce the dataset for times when MMS was on the nightside ($X_{GSM} < 0$). Following a similar approach to that from Liao et al. (2010), we exclude all the data for which the proton density was larger than 3 cm^{-3}. This is necessary because, even with the constraints mentioned above, there are times when the spacecraft was collecting data in the magnetosheath and the solar wind. Additionally, in order to exclude data collected in the lobes, a

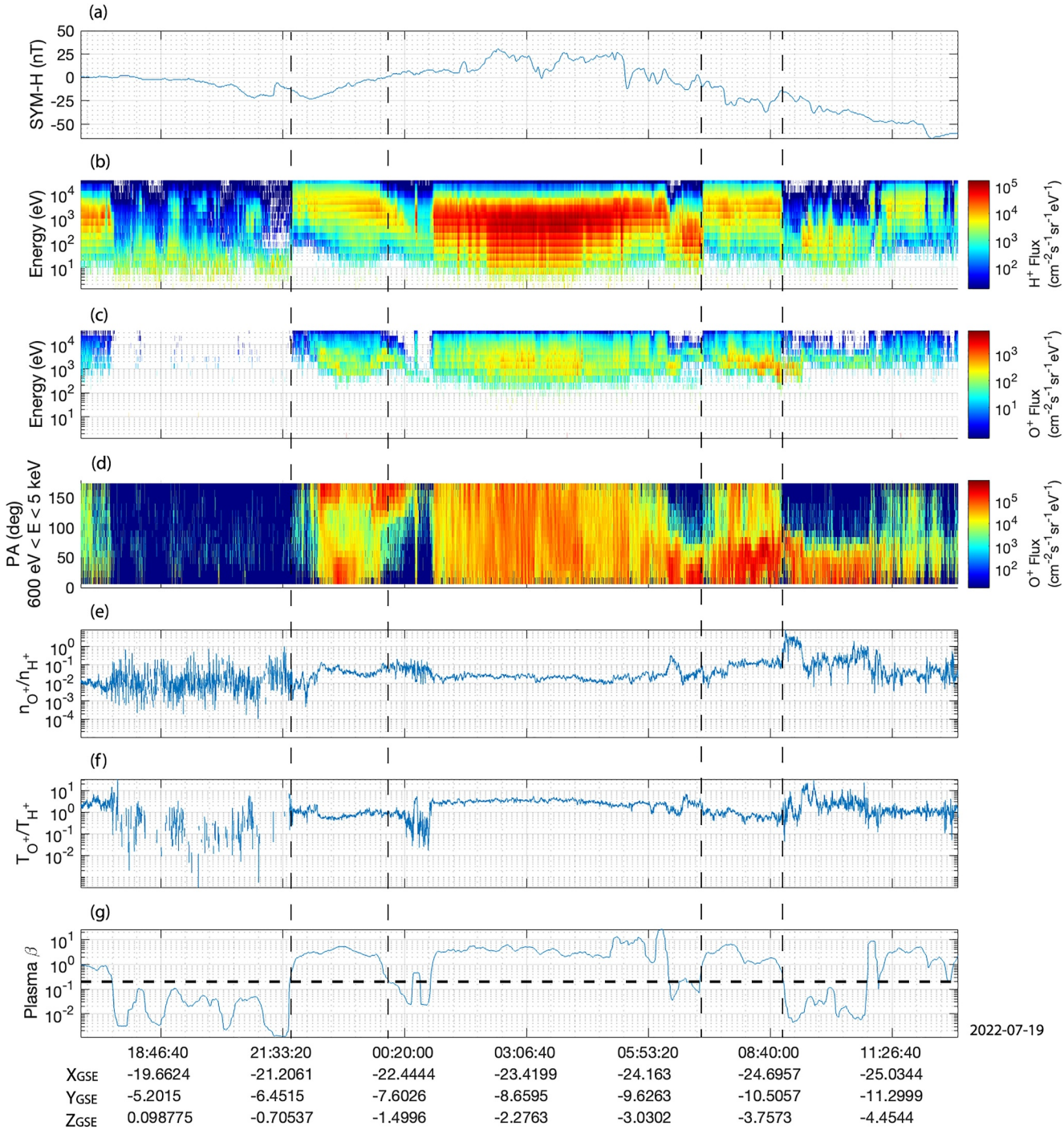

Figure 2. Data obtained during a geomagnetic storm that took place on 19 July 2022. Panel a shows the SYM-H index from the OMNI data; panels b and c show the H^+ and O^+ flux spectrograms from MMS1/HPCA; panel d shows the pitch agle distribution for O^+ for energies between 600 eV and 5 keV; panels e and f show the O^+-to H^+ density and temperature ratios; panel *g* shows the plasma beta, with the horizontal dashed line showing the boundary of 0.2 used to define the transition between plasma sheet and the lobes.

plasma beta threshold of 0.2 is imposed (i.e., $\beta > 0.2$). Finally, the moments data are averaged over 15 min by applying a moving median window, which allows the superposed epoch analysis to provide clearer trends of the plasma dynamics during the storms.

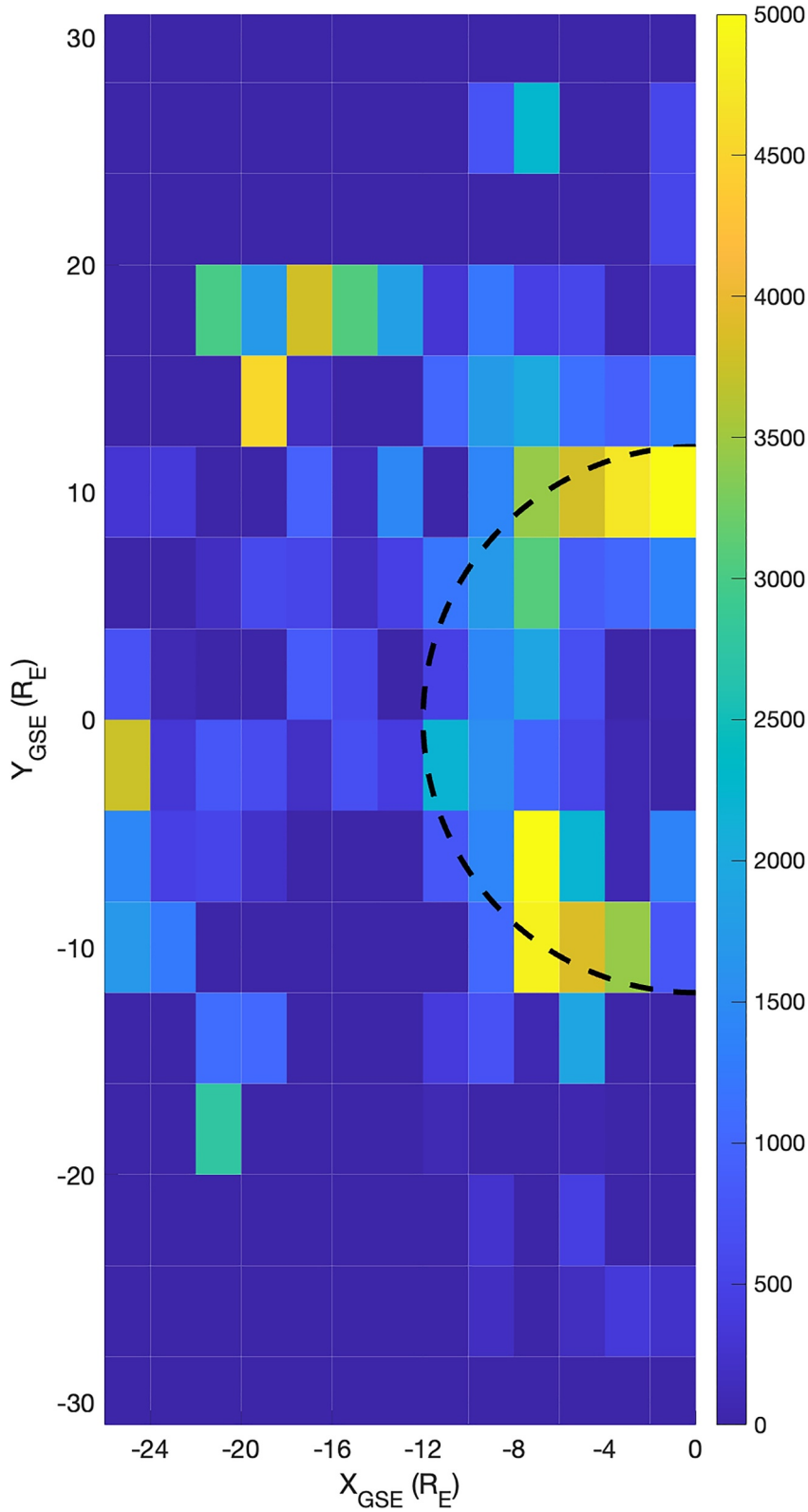

Figure 3. Number of datapoints by location (details in text). The dashed line marks the division between the two radial distance bins used in the analyses presented in Section 4.

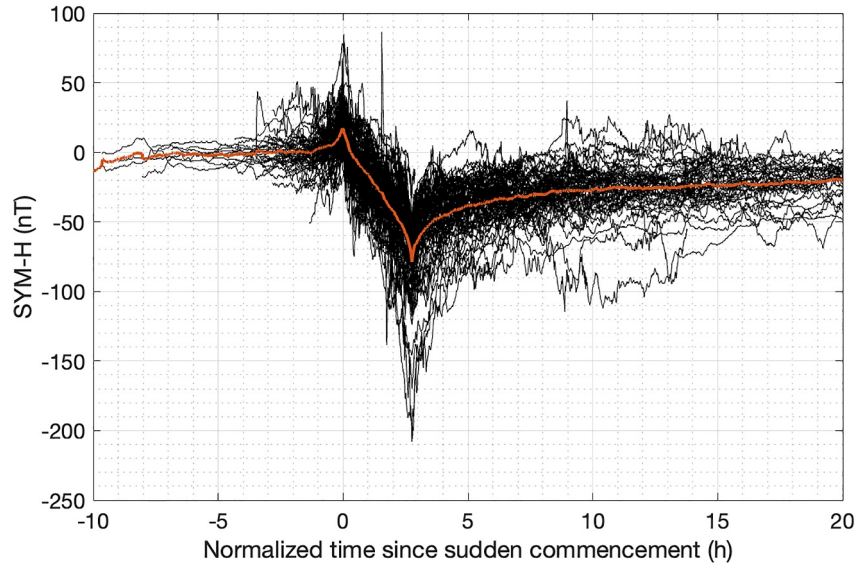

Figure 4. SYM-H index for the 90 storms considered in this study. The thin gray lines show the index for each individual storm, while the thick orange line shows the median of all the storms.

Using the subset of MMS data based on the above description, we perform a superposed epoch analysis of the density and temperature of both O^+ and H^+ ions. The data are divided between those collected at two radial distance bins, namely larger than 12 R_E and smaller than 12 R_E. This was done since MMS spatial coverage does not allow further separation between local times and radial distances without compromising the statistical robustness of the results.

Figure 3 shows the equatorial projection, in geocentric solar ecliptic (GSE) coordinates, of MMS nightside spatial coverage during the period considered in this study. MMS has a good coverage of the equatorial region, but due to its elliptical orbit with high apogee, the radial and azimuthal coverage is still relatively limited, especially for radial distances larger than 12 on the dusk sector of the magnetosphere.

Since we are interested in the evolution of the O^+ population throughout the duration of geomagnetic storms, the maximum of the SYM-H index during the sudden commencement, before the main phase of the storms, is used as starting point for the superposed epoch analysis. In order to understand the dynamics of the outflowing ions during the main phase of the storm, we align the minima of the storms, effectively applying a factor to the time arrays of each of the storms. Due to this alignment, the time axis for the plots presented in this section is referred to as normalized time.

We then focus on the first 20 hr of the storms, effectively meaning that the dynamics during the main phase of the geomagnetic storms are analyzed. For the purpose of understanding the dynamics of the ion populations prior to the beginning of the storms, we also include 10 hr of data before sudden commencement (these times are shown as negative values in the superposed epoch analysis plots). Figure 4 shows a plot of the SYM-H index for the 90 storms included in the statistical analysis, with the thick orange line showing the median values.

4. Results

For each figure in this section, each data point (orange squares) corresponds to the median of the data over taken over the 15-min window, while the error bars correspond to the median absolute deviation (MAD) of the samples. This is defined as the median of the absolute deviations from the median of the data ($\tilde{X}$), divided by the square root of the number of samples (n) (Equation 1). To better illustrate the trends, a black dashed line shows the data smoothed with a Savitzky-Golay filter (Savitzky & Golay, 1964).

$$\mathrm{MAD} = \left(\mathrm{median}\left(|X_i - \tilde{X}|\right)\right)/\sqrt{n} \quad (1)$$

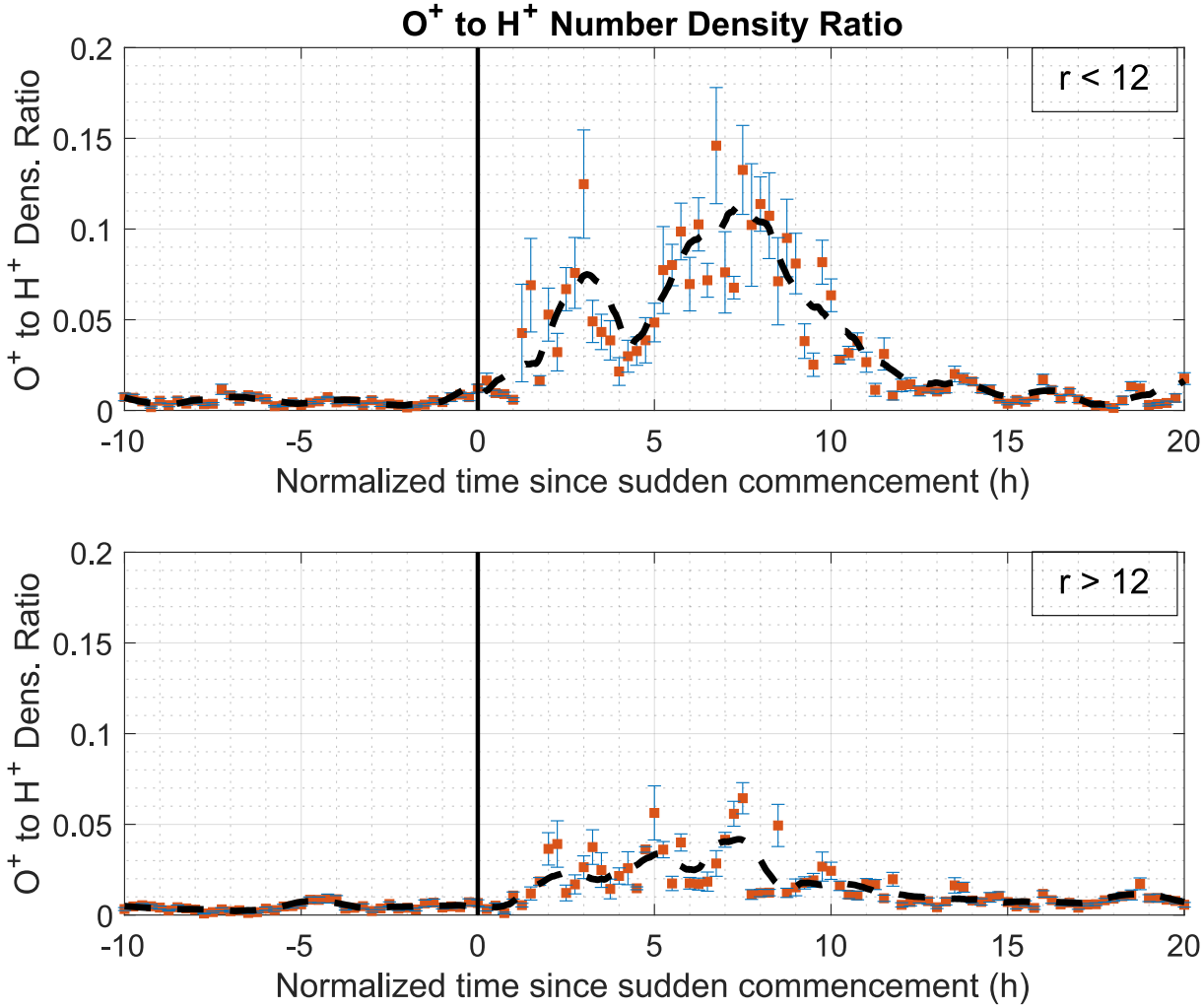

Figure 5. O^+ to H^+ number density ratio for all the 90 storms, superposed with the corresponding time since the beginning of the storm ($t = 0$).

4.1. Number Density

Figure 5 shows the O^+-to-H^+ density ratio (defined as the ratio of the corresponding medians as defined at the beginning of this section) for the first 10 hr prior to sudden commencement and the first 20 hr of the geomagnetic storm, as measured at radial distances smaller (top) and larger (bottom) than 12 R_E. We used the density ratio to highlight the possible differences in the evolution of the two populations corresponding to different sources (ionospheric for O^+ vs. solar wind and ionospheric for H^+), as the geomagnetic storm progresses.

Before sudden commencement, the ion population in the plasma sheet closer to Earth is dominated by H^+, with the ratio being consistently low. At the very beginning of the storm, right after the initial compression indicated by the sudden commencement, the ratio in the inner magnetosphere starts to increase, almost coincident with the sudden commencement. This increase in the ratio is further enhanced in a subsequent peak occurring at around 7 hr after sudden commencement. After this, the increase in the O^+ relaxes before reaching levels similar the ones observed before the storm.

Farther from Earth, the ratios are similar pre-storm, and shortly after sudden commencement, with a small delay of about an hour, an increase in the ratio is observed for a few hours, almost coincident with the increase observed closer to Earth, although at significantly lower values. This smaller increase, with a small delay at the beginning, is consistent with accelerated ions traveling further along the tail before entering the plasma sheet.

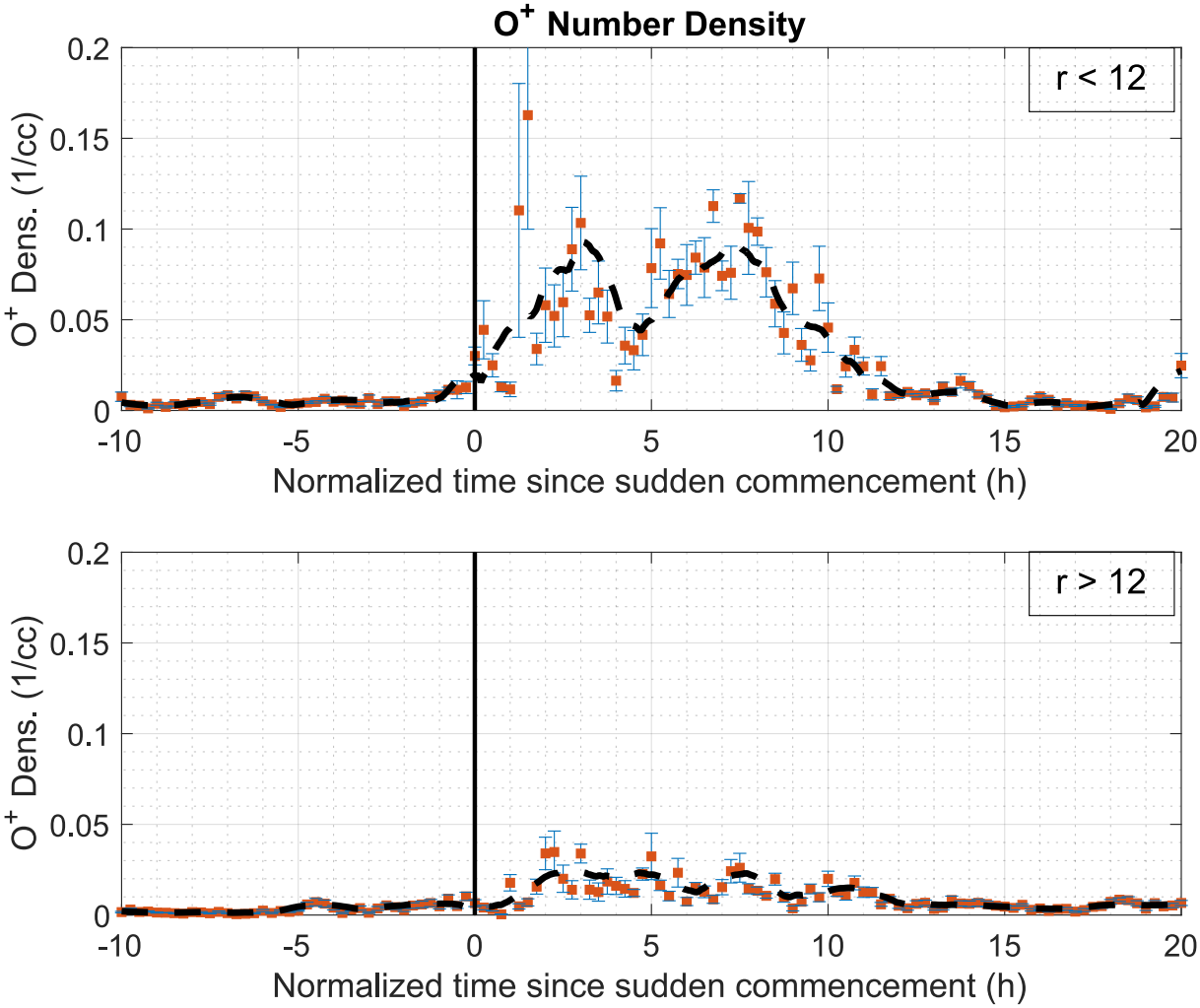

Figure 6. O^+ number density for all the 90 storms, superposed with the corresponding time since the beginning of the storm ($t = 0$).

These trends show a clear enhancement of the O^+ to H^+ ratio closer to Earth, indicating a more direct access of fresh O^+ ions from the ionosphere, rather than being brought inwards by magnetospheric convection. This interpretation is supported by the fact that the increase in the ratio is due to an increase in the O^+ density, and not due to changes in the H^+ density, as shown in the individual density plots presented in Figures 6 and 7. Interestingly, for both radial distance bins, an increase in the H^+ density is observed for a few hours before sudden commencement, possibly due to enhanced activity arising from a slow compression of the magnetosphere.

The results from the number density ratio are in agreement with what was reported by Ohtani et al. (2011), showing an increase in the O^+ to H^+ ratio with decreasing radial distance. The data used in this study, spanning from 2016 to 2022, correspond to the decreasing phase of solar cycle 24, solar minimum and the start of solar cycle 25. Ohtani et al. (2011) found number density ratios of approximately 0.02–0.04 closer to Earth, and approximately 0.01–0.02 farther from Earth, for what they labeled as minimum and median solar activity (Figure 8 in their study). We observe similar values at the beginning and at the end of the 10-hr period analyzed, with significantly larger ratios closer to Earth. This increase is due to the dynamics of the O^+ ions of ionospheric origin being extracted as the geomagnetic storm progresses, and it can only be observed when performing a superposed epoch analysis like the one performed here.

Due to the previously mentioned issue with the compression algorithm used during collection of the data, part of the low-energy ions have been removed. In general, this issue is expected to affect O^+ more than H^+ (due to the

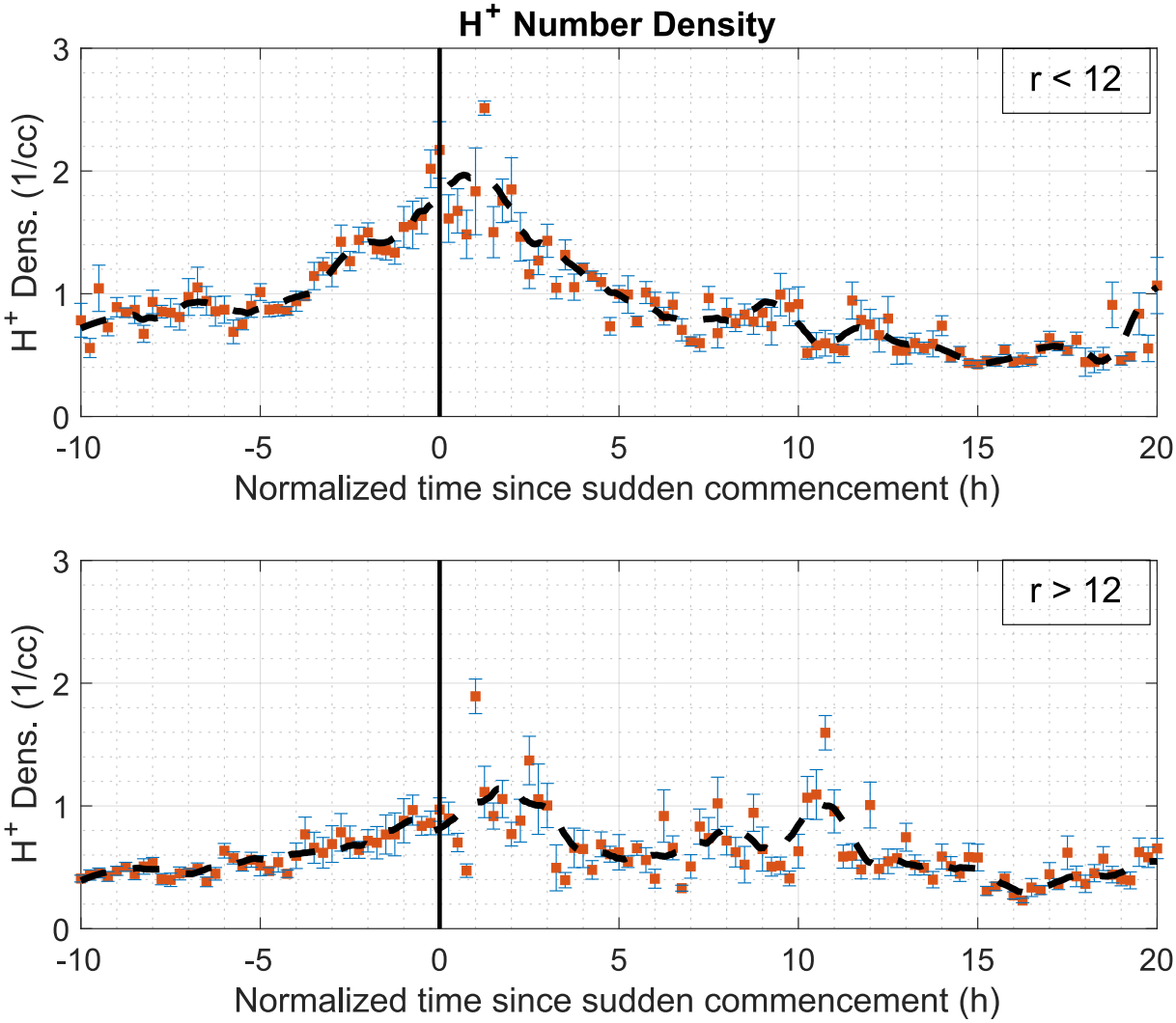

Figure 7. H^+ number density for all the 90 storms, superposed with the corresponding time since the beginning of the storm ($t = 0$).

lower densities), meaning that the ratios presented in Figure 5 are expected to be a lower limit to the actual ones present in the magnetosphere during active times.

4.2. Scalar Temperature

Figures 8 and 9 show the O^+ and H^+ scalar temperatures in a similar organization as Figure 5. For O^+ closer to Earth, the overall trend of the temperature is stable over the whole period being analyzed, with slow fluctuations between 4 and 5 keV, with higher variability before the storm, and a tendency to stabilize after sudden commencement. Farther from Earth, the observed O^+ is colder than closer to Earth before the beginning of the storm, and it increases over the first few hours, staying stable at about 4 keV afterward during the recovery period.

For H^+ closer to Earth, an increase in the temperature is observed right around sudden commencement, and the temperatures remain elevated throughout the 20 hr after the sudden commencement. Farther from Earth, an increase is also observed, although with a delay of a couple of hours after sudden commencement, and significant variability during the rest of the 20 hr being analyzed. The increase in the H^+ temperature is faster than that observed for O^+. This difference in time is consistent with the presence of the velocity filter effect, where lighter ions are transported toward the tail faster than heavier ions with the same energy.

For the individual temperatures (Figures 8 and 9) the results from the superposed epoch analysis are not as clear as those for the densities. Ohtani et al. (2011) found an increase in the temperatures for both H^+ and O^+ ions with

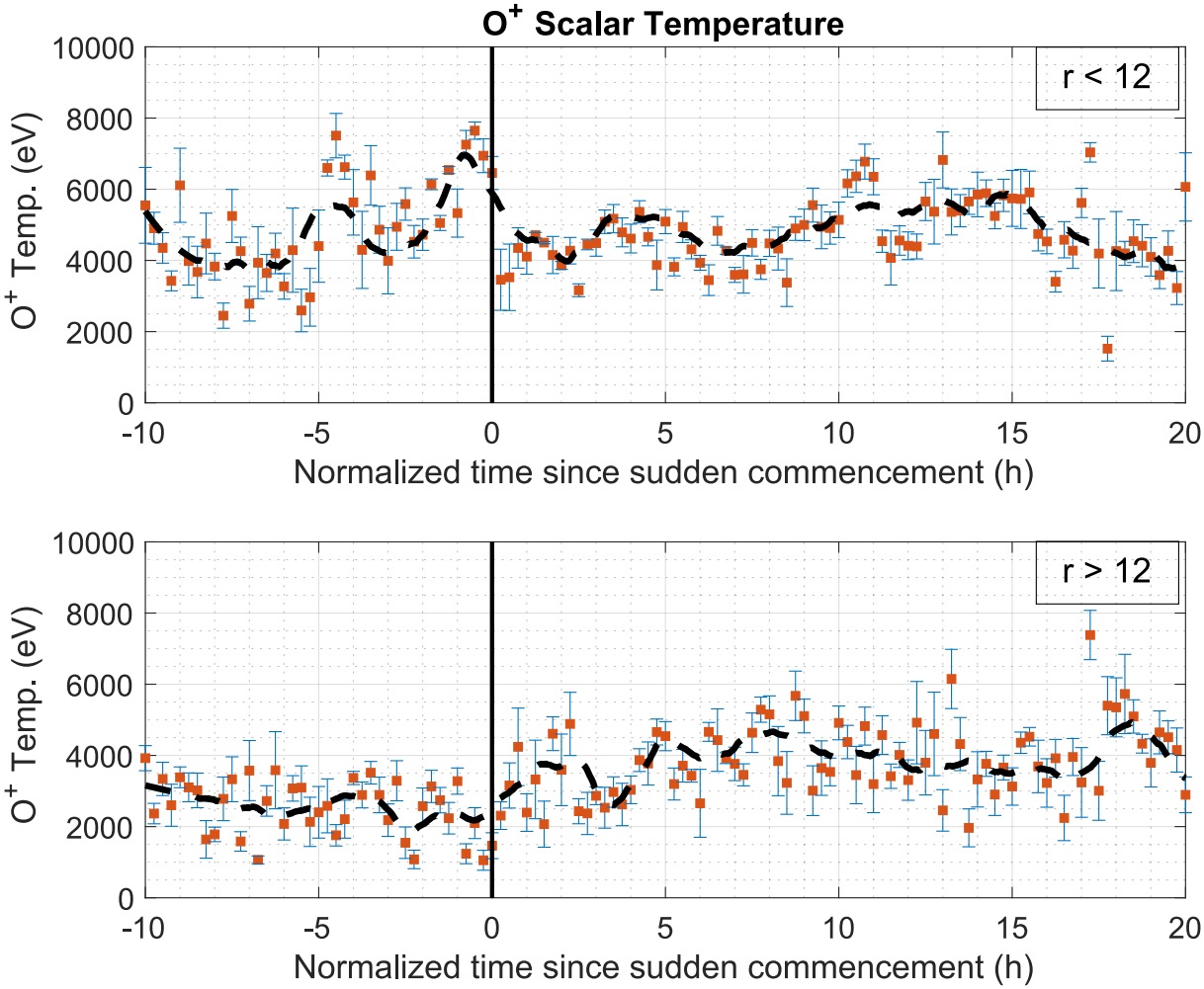

Figure 8. O^+ scalar temperature for all the 90 storms, superposed with the corresponding time since the beginning of the storm.

increasing storm activity (Figure 7 in their study), with a more pronounced change for H^+. Since we are combining all the 90 storms into a single superposed epoch analysis, this trend with geomagnetic activity will not be evident in our results. We do see an enhancement in the temperatures for O^+ ions farther from Earth, and for H^+ at both radial distance bins, and these enhancements could be explained as acceleration of the outflowing ions as the storm progresses.

Ohtani et al. (2011) also reported an increase (decrease) in O^+ (H^+) temperature with increasing radial distance, interpreting this as a result of ionospheric O^+ being accelerated when transported toward the distant plasma sheet, and H^+ being transported inwards during substorm dipolarization events and accelerated along the way (Millan & Baker, 2012). Our analysis shows the same results for the case of H^+, but the opposite for O^+, with higher temperatures closer to Earth before sudden commencement, which could be partly explained by the overall lack of O^+ in the outer magnetosphere prior to the beginning of the storms (as evident from Figure 6), or the limited statistics of the dataset. The temperatures reach similar values at both radial distance bins as the storm progresses. One caveat to consider is that for periods when the measured O^+ is very low, the calculation of the temperatures yields a value that is higher than in reality (by artificially removing the colder populations), so in general, it is difficult to derive specific conclusions from this particular dataset.

5. Conclusions

After performing a superposed epoch analysis of plasma moments derived from data collected by the HPCA instrument aboard MMS 1 during 90 geomagnetic storms, we have found evidence of enhanced ionospheric O^+

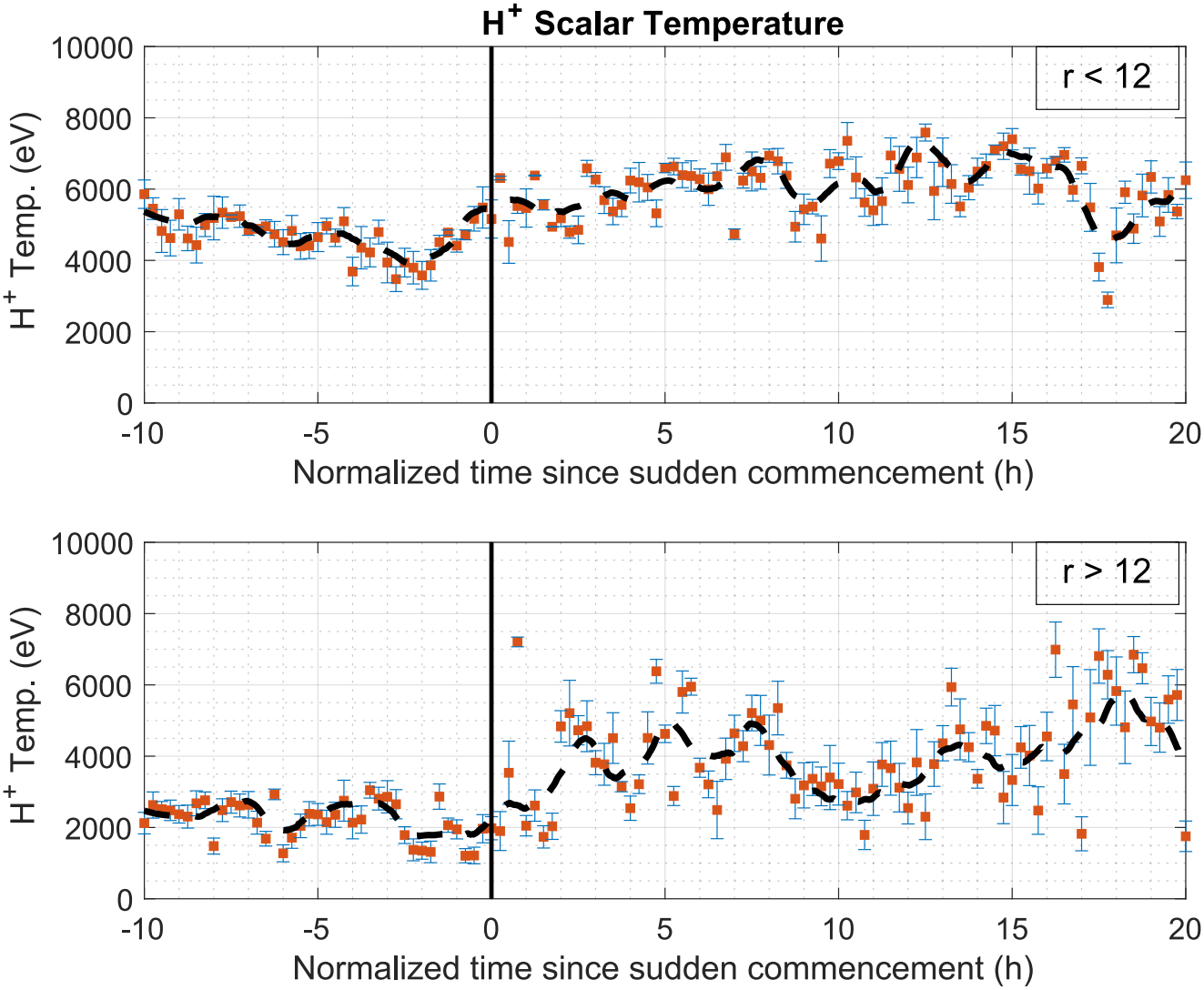

Figure 9. H^+ scalar temperature for all the 90 storms, superposed with the corresponding time since the beginning of the storm.

access to the plasma sheet at radial distances lower than 12 R_E, with a significantly smaller increase in the relative O^+ abundance at larger radial distances. To investigate the difference between storm and non-storm time, we focused on the 10-hr period before (non-storm) and on the 20-hr period after (storm) the sudden commencement. This separation covers both a quiet period, and the main phase of the analyzed storms. Closer to Earth ($L < 12$), a marked increase in the O^+ to H^+ density ratio is observed for the first 12 hr of the storm, before decreasing to pre-storm values.

At radial distances larger than 12 R_E, the number density ratio remains significantly less perturbed, with an increase starting at around 1 hr after the beginning of the storm, and lasting for about 10 hr. This delay of an hour could indicate that the O^+ observed farther from Earth is originated in the dayside cusp, and is being transported along together with the field lines being convicted toward the nightside. Additionally, some of this could be caused by convection from the distant tail, at distances not covered by MMS. The original enhancement of O^+ densities farther from Earth is observed (in Figure 6) at around 2 hr after sudden commencement, which is very close to the expected value for a 100 eV O^+ ion of 1.5 hr to reach radial distances of approximately 20 R_E, as estimated by Kistler et al. (2016).

Temperature data derived from HPCA measurements is especially affected by the compression algorithm being used, which complicates the analysis of the temperature trends. The results are partially in good agreement with

previous studies (e.g., Ohtani et al., 2011), regarding the increase in temperature for H^+ with increasing radial distance, but the opposite is found for O^+. At radial distances larger than 12 R_E, both ion populations see an increase in the scalar temperatures, with the enhancement happening approximately 2 hr earlier for H^+ than for O^+, which seems to indicate that the heating of the outflowing populations is happening while the ions are being transported tailwards, and the time difference arises from the velocity filter effect. The combination of an increase in the H^+ ion densities and cold temperatures at both radial bins is in good agreement with previous studies that have shown a dense and cold plasma sheet prior to geomagnetic storms using data analysis(e.g. Kistler, 2020) and test particle simulations (e.g., Ebihara et al., 2006).

Data Availability Statement

The MMS data used in the study are available from the MMS Science Data Center (https://lasp.colorado.edu/mms/sdc/public/data). Data analysis was performed using custom-prepared Matlab software (for the superposed epoch analysis) and SPEDAS Angelopoulos et al. (2019).

Acknowledgments
This research was funded by the NASA grant NNX17AI54G. SR acknowledge support by the NASA DRIVE Science Center for Geospace Storms (CGS) under award 80NSSC22M0163.

References

Angelopoulos, V., Baumjohann, W., Kennel, C. F., Coronti, F. V., Kivelson, M. G., Pellat, R., et al. (1992). Bursty bulk flows in the inner central plasma sheet. *Journal of Geophysical Research (Space Physics)*, *97*(A4), 4027–4039. https://doi.org/10.1029/91JA02701

Angelopoulos, V., Cruce, P., Drozdov, A., Grimes, E. W., Hatzigeorgiu, N., King, D. A., et al. (2019). The Space Physics Environment data analysis System (SPEDAS) [Software]. *Space Science Reviews*, *215*(1), 9. https://doi.org/10.1007/s11214-018-0576-4

Ebihara, Y., Yamada, M., Watanabe, S., & Ejiri, M. (2006). Fate of outflowing suprathermal oxygen ions that originate in the polar ionosphere. *Journal of Geophysical Research (Space Physics)*, *111*(A4), A04219. https://doi.org/10.1029/2005JA011403

Gkioulidou, M., Ohtani, S., Ukhorskiy, A. Y., Mitchell, D. G., Takahashi, K., Spence, H. E., et al. (2019). Low-energy (¡keV) O^+ ion outflow directly into the inner magnetosphere: Van Allen probes observations. *Journal of Geophysical Research (Space Physics)*, *124*(1), 405–419. https://doi.org/10.1029/2018JA025862

Hamilton, D. C., Gloeckler, G., Ipavich, F. M., Stüdemann, W., Wilken, B., & Kremser, G. (1988). Ring current development during the great geomagnetic storm of February 1986. *Journal of Geophysical Research (Space Physics)*, *93*(A12), 14343–14355. https://doi.org/10.1029/JA093iA12p14343

Kistler, L. M. (2020). Ionospheric and solar wind contributions to the storm-time near-Earth plasma sheet. *Geophysical Research Letters*, *47*(23), e90235. https://doi.org/10.1029/2020GL090235

Kistler, L. M., Hamilton, D. C., Ipavich, F. M., & Gloeckler, G. (1989). The ion energy spectra in the ring current during the geomagnetic storm of February, 1986. *Advances in Space Research*, *9*(12), 183–186. https://doi.org/10.1016/0273-1177(89)90327-X

Kistler, L. M., Mouikis, C. G., Asamura, K., Yokota, S., Kasahara, S., Miyoshi, Y., et al. (2019). Cusp and nightside auroral sources of O^+ in the plasma sheet. *Journal of Geophysical Research (Space Physics)*, *124*(12), 10036–10047. https://doi.org/10.1029/2019JA027061

Kistler, L. M., Mouikis, C. G., Klecker, B., & Dandouras, I. (2010). Cusp as a source for oxygen in the plasma sheet during geomagnetic storms. *Journal of Geophysical Research (Space Physics)*, *115*(A3), A03209. https://doi.org/10.1029/2009JA014838

Kistler, L. M., Mouikis, C. G., Spence, H. E., Menz, A. M., Skoug, R. M., Funsten, H. O., et al. (2016). The source of O^+ in the storm time ring current. *Journal of Geophysical Research (Space Physics)*, *121*(6), 5333–5349. https://doi.org/10.1002/2015JA022204

Kronberg, E. A., Ashour-Abdalla, M., Dandouras, I., Delcourt, D. C., Grigorenko, E. E., Kistler, L. M., et al. (2014). Circulation of heavy ions and their dynamical effects in the magnetosphere: Recent observations and models. *Space Science Reviews*, *184*(1–4), 173–235. https://doi.org/10.1007/s11214-014-0104-0

Liao, J., Kistler, L. M., Mouikis, C. G., Klecker, B., Dandouras, I., & Zhang, J. C. (2010). Statistical study of O^+ transport from the cusp to the lobes with Cluster CODIF data. *Journal of Geophysical Research (Space Physics)*, *115*(A12), A00J15. https://doi.org/10.1029/2010JA015613

Liu, Z.-Y., & Zong, Q.-G. (2022). Ionospheric oxygen outflows directly injected into the inner magnetosphere: Van allen probes statistics. *Journal of Geophysical Research: Space Physics*, *127*(10), e2022JA030611. https://doi.org/10.1029/2022JA030611

Lui, A. T. Y. (1991). Plasma transport in the Earth's magnetotail. *Geophysical Monograph Series*, *62*, 41–53. https://doi.org/10.1029/GM062p0041

Maggiolo, R. (2015). *Auroral dynamics and space weather. Auroral arcs and ion outflow* (pp. 39–58). American Geophysical Union. https://doi.org/10.1002/9781118978719.ch4

Millan, R. M., & Baker, D. N. (2012). Acceleration of particles to high energies in earth's radiation belts. *Space Science Reviews*, *173*(1–4), 103–131. https://doi.org/10.1007/s11214-012-9941-x

Mitchell, D. G., Brandt, P. C. s., & Mende, S. B. (2005). Oxygen in the ring current during major storms. *Advances in Space Research*, *36*(10), 1758–1761. https://doi.org/10.1016/j.asr.2004.03.025

Mitchell, D. G. C., Son Brandt, P., Roelof, E. C., Hamilton, D. C., Retterer, K. C., & Mende, S. (2003). Global imaging of O^+ from IMAGE/HENA. *Space Science Reviews*, *109*(1), 63–75. https://doi.org/10.1023/B:SPAC.0000007513.55076.00

Nosé, M., Keika, K., Kletzing, C. A., Spence, H. E., Smith, C. W., MacDowall, R. J., et al. (2016). Van Allen Probes observations of magnetic field dipolarization and its associated O^+ flux variations in the inner magnetosphere at L ¡ 6.6. *Journal of Geophysical Research (Space Physics)*, *121*(8), 7572–7589. https://doi.org/10.1002/2016JA022549

Ohtani, S., Nosé, M., Christon, S. P., & Lui, A. T. Y. (2011). Energetic O^+ and H^+ ions in the plasma sheet: Implications for the transport of ionospheric ions. *Journal of Geophysical Research (Space Physics)*, *116*(A10), A10211. https://doi.org/10.1029/2011JA016532

Pitkänen, T., Chong, G. S., Hamrin, M., Kullen, A., Karlsson, T., Park, J. S., et al. (2023). Statistical survey of magnetic forces associated with earthward bursty bulk flows measured by MMS 2017-2021. *Journal of Geophysical Research (Space Physics)*, *128*(5), e2022JA031094. https://doi.org/10.1029/2022JA031094

Savitzky, A., & Golay, J. E. (1964). Smoothing and differentiation of data by simplified least squares procedures. *Analytical Chemistry*, *36*(8), 1627–1639. https://doi.org/10.1021/ac60214a047

Strangeway, R. J., Ergun, R. E., Su, Y. J., Carlson, C. W., & Elphic, R. C. (2005). Factors controlling ionospheric outflows as observed at intermediate altitudes. *Journal of Geophysical Research (Space Physics)*, *110*(A3), A03221. https://doi.org/10.1029/2004JA010829

Young, D. T., Burch, J. L., Gomez, R. G., De Los Santos, A., Miller, G. P., Wilson, P., et al. (2016). Hot plasma composition analyzer for the magnetospheric multiscale mission. *Space Science Reviews*, *199*(1–4), 407–470. https://doi.org/10.1007/s11214-014-0119-6

Zhao, H., Li, X., Baker, D. N., Fennell, J. F., Blake, J. B., Larsen, B. A., et al. (2015). The evolution of ring current ion energy density and energy content during geomagnetic storms based on van allen probes measurements. *Journal of Geophysical Research: Space Physics*, *120*(9), 7493–7511. https://doi.org/10.1002/2015ja021533